

Categorizing the Role of Respiration in Cardiovascular and Cerebrovascular Variability Interactions

Alberto Porta*, Senior Member, IEEE, Francesca Gelpi, Vlasta Bari, Member, IEEE, Beatrice Cairo, Student Member, IEEE, Beatrice De Maria, Davide Tonon, Gianluca Rossato, Marco Ranucci, and Luca Faes, Senior Member, IEEE

Abstract— Objective: Respiration disturbs cardiovascular and cerebrovascular controls but its role is not fully elucidated. **Methods:** Respiration can be classified as a confounder if its observation reduces the strength of the causal relationship from source to target. Respiration is a suppressor if the opposite situation holds. We prove that a confounding/suppression (C/S) test can be accomplished by evaluating the sign of net redundancy/synergy balance in the predictability framework based on multivariate autoregressive modelling. In addition, we suggest that, under the hypothesis of Gaussian processes, the C/S test can be given in the transfer entropy decomposition framework as well. **Experimental protocols:** We applied the C/S test to variability series of respiratory movements, heart period, systolic arterial pressure, mean arterial pressure, and mean cerebral blood flow recorded in 17 pathological individuals (age: 64±8 yrs; 17 males) before and after induction of propofol-based general anesthesia prior to coronary artery bypass grafting, and in 13 healthy subjects (age: 27±8 yrs; 5 males) at rest in supine position and during head-up tilt with a table inclination of 60°. **Results:** Respiration behaved systematically as a confounder for cardiovascular and cerebrovascular controls. In addition, its role was affected by propofol-based general anesthesia but not by a postural stimulus of limited intensity. **Conclusion:** The C/S test can be fruitfully exploited to categorize the role of respiration over causal variability interactions. **Significance:** The application of the C/S test could favor the comprehension of the role of respiration in cardiovascular and cerebrovascular regulations.

Index Terms—Multivariate autoregressive model, redundancy, synergy, confounding, suppression, predictability decomposition, transfer entropy, cerebrovascular autoregulation, heart rate variability, general anesthesia, head-up tilt, autonomic nervous system, cardiac neural control.

This work was supported in part by the Piano Sostegno della Ricerca 2020, University of Milan, Milan, Italy, to A.P. and by Ricerca Corrente from the Italian Ministry of Health to Policlinico San Donato.

*A. Porta is with Department of Biomedical Sciences for Health, University of Milan, Milan, Italy and Department of Cardiothoracic, Vascular Anesthesia and Intensive Care, IRCCS Policlinico San Donato, San Donato Milanese, Milan, Italy (correspondence email: alberto.porta@unimi.it). F. Gelpi and B. Cairo are with Department of Biomedical Sciences for Health, University of Milan, Milan, Italy. V. Bari, and M. Ranucci are with Department of Cardiothoracic, Vascular Anesthesia and Intensive Care, IRCCS Policlinico San Donato, San Donato Milanese, Milan, Italy. B. De Maria is with IRCCS Istituti Clinici Scientifici Maugeri, Milan, Italy. D. Tonon and G. Rossato are with Department of Neurology, IRCCS Sacro Cuore Don Calabria Hospital, Negrar, Verona, Italy. L. Faes is with Department of Engineering, University of Palermo, Palermo, Italy.

I. INTRODUCTION

THE behavior of physiological systems, such as cardiovascular (CV) and cerebrovascular (CBV) systems, is the result of their complex intrinsic functioning and of the interactions with other systems supported by the neural pathways and the network of vessels [1]. The behavior of a given system, taken as the target, is usually described as a stochastic process modeling the dependence of the current state on its own past states, usually referred to as self-dependency, on past states of a system taken as a source, usually referred to as cross-dependency, and on past states of the additional systems, usually referred to as conditioning systems, blurring the relationship between source and target [2]-[6]. In the context of the description of the dynamic interactions it is important to typify the role of conditioning systems on the relationship between source and target. This categorization is useful to better understand the impact of the conditioning systems in shaping the interactions between source and target and in modulating the variety of target behaviors that might be observed in response to the same dynamics of the source.

The aim of this study is to propose a method to categorize the role of conditioning systems over the relationship between source and target. The approach allows the separation of confounding (C) and suppression (S) effects [7] via a simple C/S test. The C/S test exploits the net redundancy/synergy balance between source and conditioning systems in shaping the target dynamics [8]-[11]. It is shown that the classification of more peculiar causal schemes, corresponding to very common situations such as uncorrelated sources (US), common disturbance (CD) and mediation (M), necessitates the introduction of additional *a priori* physiological knowledge. The C/S test is applied to clarify the role of the respiratory system in modulating CV and CBV variability interactions on two experimental protocols featuring the contemporaneous recordings of the beat-to-beat variability series of heart period (HP), mean and systolic arterial pressure (MAP and SAP), mean cerebral blood flow (MCBF) and respiration (R) in patients undergoing general anesthesia with propofol and remifentanyl under mechanical ventilation [12],[13], and in

healthy subjects during postural challenge under spontaneous breathing [14]-[15]. The two protocols were considered because both general anesthesia and postural challenge modulate the state of the autonomic nervous system that has a profound impact on HP-SAP and MCBF-MAP variability interactions [12]-[15]. CV and CBV regulations have been studied extensively via both linear and nonlinear model-based techniques [16]-[22] but the impact of R on them remains poorly assessed and largely underestimated.

II. METHODS

A. Generalities and Definitions

Let us consider an ensemble of systems composed by a source, a target and a conditioning system denoted as X, Y and Z respectively. Their dynamic behavior is given by the processes $X = \{X_{n,s}, n=1, \dots, N; s \in S\}$, $Y = \{Y_{n,s}, n=1, \dots, N; s \in S\}$ and $Z = \{Z_{n,s}, n=1, \dots, N; s \in S\}$ respectively, where n is the time index, N is the overall time horizon of the process, s is the outcome of a random experiment and S is the collection of all possible outcomes. Assigned the outcome s of the random experiment to \bar{s} , $x = \{x_n = X_{n,s=\bar{s}}, n=1, \dots, N\}$, $y = \{y_n = Y_{n,s=\bar{s}}, n=1, \dots, N\}$ and $z = \{z_n = Z_{n,s=\bar{s}}, n=1, \dots, N\}$ are realizations of the processes X, Y and Z corresponding to the time series recorded during an experimental session. Assigned the time index n to \bar{n} , $X_{\bar{n}} = X_{n=\bar{n},s}$, $Y_{\bar{n}} = Y_{n=\bar{n},s}$ and $Z_{\bar{n}} = Z_{n=\bar{n},s}$ represent the states of the systems X, Y and Z respectively at the time $n = \bar{n}$. Assigned the time index n to \bar{n} and the outcome s of the random experiment to \bar{s} , $x_{\bar{n}} = X_{n=\bar{n},s=\bar{s}}$, $y_{\bar{n}} = Y_{n=\bar{n},s=\bar{s}}$ and $z_{\bar{n}} = Z_{n=\bar{n},s=\bar{s}}$ are samples of the realization x , y and z at time \bar{n} . Let us suppose that X, Y and Z are ergodic processes such a way their statistical properties are invariant under time shift and can be estimated via temporal averaging instead of ensemble averaging. Being ergodic, X, Y and Z are stationary as well. Let us also hypothesize that X, Y and Z are Gaussian processes with zero mean and unit variance obtained by subtracting the mean and by dividing the deviation of each value from the mean by the standard deviation.

B. Description of the Effect of the Conditioning System on the Dynamic Interactions between Source and Target

Let us consider the universe of knowledge Ω formed by the dynamic behaviors of the source, target and conditioning systems, i.e. $\Omega_{XYZ} = \{X, Y, Z\}$, and three restricted universes built by considering separately X and Z together with Y, i.e. $\Omega_{XY} = \{X, Y\} = \Omega_{XYZ} \setminus \{Z\}$ and $\Omega_{YZ} = \{Y, Z\} = \Omega_{XYZ} \setminus \{X\}$, and the target alone, i.e. $\Omega_Y = \{Y\} = \Omega_{XYZ} \setminus \{X, Z\}$. In Ω_{XYZ} the effect of the conditioning system on the dynamic interactions between the source and the target is described as an autoregressive (AR) process over Y with double exogenous (X) inputs, namely X and Z, (AR_YX_{XZ}) [5], [23], [24] as

$$Y_n = a^{XYZ} \cdot Y_n^- + b^{XYZ} \cdot X_n^- + c^{XYZ} \cdot Z_n^- + W_n^{XYZ}, \quad (1)$$

where $a^{XYZ} = |a_1 \dots a_p|$, $b^{XYZ} = |b_1 \dots b_p|$ and $c^{XYZ} = |c_1 \dots c_p|$ are the vectors of constant coefficients with dimension $1 \times p$, $Y_n^- = |Y_{n-1} \dots Y_{n-p}|^T$, $X_n^- = |X_{n-\tau_X} \dots Y_{n-\tau_X-p+1}|^T$ and $Z_n^- = |Z_{n-\tau_Z} \dots Z_{n-\tau_Z-p+1}|^T$ are the vectors of the past states of Y, X and Z with dimension $p \times 1$, W_n^{XYZ} is the current state of the zero mean Gaussian white noise W^{XYZ} with variance λ_{XYZ}^2 , τ_X and τ_Y represent the latencies of the actions of X and Z on Y, and p is the model order. Analogously, we describe the dynamic dependence of Y on X in Ω_{XY} as an AR process over Y with single X input, namely X, (AR_YX_X) as

$$Y_n = a^{XY} \cdot Y_n^- + b^{XY} \cdot X_n^- + W_n^{XY}, \quad (2)$$

the dynamic influence of Z on Y in Ω_{YZ} as an AR process over Y with single Z input, namely Z, (AR_YX_Z) as

$$Y_n = a^{YZ} \cdot Y_n^- + c^{YZ} \cdot Z_n^- + W_n^{YZ}, \quad (3)$$

and the dynamics of Y in Ω_Y as an AR process over Y (AR_Y) as

$$Y_n = a^Y \cdot Y_n^- + W_n^Y, \quad (4)$$

with symbols having the same meaning as in (1) and W^{XY} , W^{YZ} and W^Y having variances λ_{XY}^2 , λ_{YZ}^2 and λ_Y^2 respectively.

C. Definition of C and S and their Link with M and CD

When considering the role of Z over a causal relationship from X to Y, namely $X \rightarrow Y$, we can classify two main typologies: C and S. In the case of C the enlargement of Ω_{XY} with the inclusion of Z reduces the predictability of Y on X. This situation implies that the portion of the Y variance explained by X in Ω_{XYZ} is smaller than that in Ω_{XY} . Conversely, in the case of S, the opposite situation is observed with the portion of the Y variance explained by X in Ω_{XYZ} that is larger than the one in Ω_{XY} . When examining the role of Z over the $X \rightarrow Y$ link, C and S should be considered the main typologies because this classification holds regardless of the type of the causal interactions linking X and Y to Z. Figure 1 summarizes all the possibilities of causal schemes concerning the role of Z on $X \rightarrow Y$. These possibilities comprise all possible types of interaction of Z over X and Y, namely unidirectional (one arrow), bidirectional (two arrows) and no link (dotted line), thus forming the most general configuration (Fig.1a). The

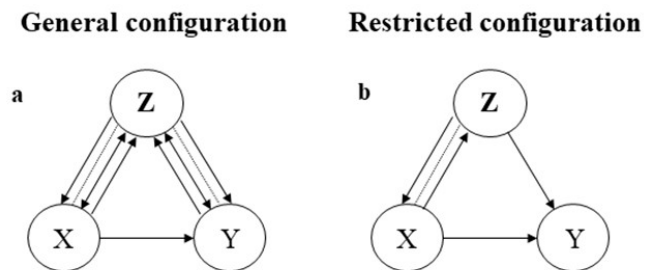


Fig.1. Sketch of all possible causal interferences of Z over the casual link from X to Y (a) and its reduction by excluding situations of bidirectional interactions and lack of directed influences of Z on Y (b).

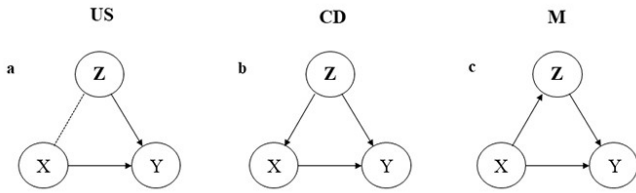


Fig.2. Sketch of all possible causal interferences of Z over the casual link from X to Y in the case of the restricted configuration reported in Fig.1b: US (a), CD (b) and M (c).

general configuration is restricted by excluding bidirectional influences between Z and X and between Z and Y. Also situations featuring no directed action from Z to Y are excluded given that Z is considered to be a source disturbing Y, thus leading to the restricted configuration summarized in Fig.1b. The schemes shown in Fig.1b are unfolded in Fig.2. The common denominator of the three patterns is the causal links from X to Y and from Z to Y. In the scheme reported in Fig.2a Z exclusively acts on Y as no link between X and Z is present, thus leading to an uncorrelation between the two sources X and Z. This configuration is labelled as uncorrelated sources (US). The scheme sketching the joint actions of Z on both X and Y is given in Fig.2b. This configuration is referred to as common driving (CD). In the scheme reported in Fig.2c Z acts as a mediator between X and Y and this configuration is labelled as mediation (M).

D. Toward a C/S test

In this study we exploited the predictability decomposition framework [9], [10] to classify the influence of Z on the causal relationship from X to Y. In this framework causal predictability (CP) from X to Y is defined as

$$CP_{X \rightarrow Y} = \sigma_Y^2 - \sigma_{XY}^2, \quad (5)$$

where σ_Y^2 and σ_{XY}^2 represent the variance of the prediction error of the model AR_Y and $AR_Y X_X$ being an estimate of the variances λ_Y^2 and λ_{XY}^2 of W^Y and W^{XY} respectively. $CP_{X \rightarrow Y}$ represents the decrement of unpredictability of Y when X is observed, namely the fraction of the variance of Y genuinely explained by X in Ω_{XY} .

In the predictability decomposition framework [10] CP from X to Y given Z is defined as

$$CP_{X \rightarrow Y|Z} = \sigma_{YZ}^2 - \sigma_{YXZ}^2, \quad (6)$$

where σ_{YZ}^2 and σ_{YXZ}^2 represent the variance of the prediction error of the model $AR_Y X_Z$ and $AR_Y X_{XZ}$ being an estimate of the variances λ_{YZ}^2 and λ_{YXZ}^2 of W^{YZ} and W^{YXZ} respectively. $CP_{X \rightarrow Y|Z}$ represents the decrement of unpredictability of Y when X is observed above and beyond the contribution of Z, namely the fraction of the variance of Y genuinely explained by X in Ω_{XYZ} . According to Sect.IIC Z is a confounder for $X \rightarrow Y$ if

$$CP_{X \rightarrow Y} > CP_{X \rightarrow Y|Z}, \quad (7)$$

because the inclusion of Z in Ω_{XY} reduces the ability of predicting Y when X is observed given that Z is capable to explain a sizable portion of the variance of Y. Conversely, if

$$CP_{X \rightarrow Y} < CP_{X \rightarrow Y|Z}, \quad (8)$$

Z is a suppressor because the enlargement of Ω_{XY} with Z increases the ability of predicting Y via X. Given this observation a test for detecting C/S is simply based on the assessment of the sign of the difference $CP_{X \rightarrow Y} - CP_{X \rightarrow Y|Z}$.

E. Testing C/S via Net Redundancy/Synergy Balance

In the predictability decomposition framework [10] the interactive predictability (IP) of X and Z to Y is defined as

$$IP(Y; X, Z) = CP_{X \rightarrow Y} + CP_{Z \rightarrow Y} - CP_{X, Z \rightarrow Y}. \quad (9)$$

$IP(Y; X, Z)$ has the notable property of assessing the difference between redundancy and synergy of X and Z to Y, namely the so-called net redundancy/synergy balance [9], [10], [25], [26]. Indeed, in agreement with the theoretical definition of redundancy when $IP(Y; X, Z) > 0$ the sum of the ability of X and Z in predicting Y, when X and Z are individually considered, is greater than the ability of X and Z in predicting Y when X and Z are considered together, thus indicating a prevalent redundancy of X and Z to Y. Conversely, in agreement with the theoretical definition of synergy, the opposite situation, namely $IP(Y; X, Z) < 0$, indicates a prevalent synergy. Given that $IP(Y; X, Z)$ can be positive or negative, $IP(Y; X, Z)$ is valuable to assess the net redundancy/synergy balance, while it is useless to assess redundancy and synergy in isolation without introducing additional relations [2], [8].

Since the amount of Y variance that can be explained using the past of X and Z above and beyond the portion that can be derived from the past of Y can be calculated as the decrement of unpredictability when Y is described in Ω_{XYZ} compared to Ω_Y [10] as

$$CP_{X, Z \rightarrow Y} = \sigma_Y^2 - \sigma_{YXZ}^2, \quad (10)$$

where σ_{YXZ}^2 represents the variance of the prediction error of the regression of Y on its own past and the past of X and Z, the application of the (5), (6) and (10) leads one to

$$IP(Y; X, Z) = CP_{X \rightarrow Y} - CP_{X \rightarrow Y|Z}, \quad (11)$$

thus testing C/S via the assessment of the sign of $IP(Y; X, Z)$.

By following the duality between predictability [9], [10] and transfer entropy (TE) [4], [8] [10], [11], [27]-[29] decomposition frameworks holding for Gaussian random variables [3], it can be easily proved that the C/S test can be carried out by assessing the sign of interactive TE (ITE) computed as

$$ITE(Y; X, Z) = 0.5 \cdot \log \frac{\sigma_Y^2 \cdot \sigma_{YXZ}^2}{\sigma_{XY}^2 \cdot \sigma_{YZ}^2}, \quad (12)$$

where log is the natural logarithm [10]. This relation follows from the definition $ITE(Y; X, Z) = TE_{X \rightarrow Y} - TE_{X \rightarrow Y|Z}$, where the TEs are defined similarly to (5) and (6) in terms of entropies as $TE_{X \rightarrow Y} = H_Y - H_{XY}$ and $TE_{X \rightarrow Y|Z} = H_{YZ} - H_{YXZ}$, and for Gaussian variables each entropy term H is a function of the corresponding residual variance σ^2 , i.e. $H = 0.5 \cdot \log(2\pi e \sigma^2)$ [3].

F. Generalization of the C/S Test to Vector Variables

Let us imagine to evaluate the role of $\mathbf{Z}=[Z_1, \dots, Z_k]$, where \mathbf{Z} is a vector variable of dimension $1 \times k$, collecting k stochastic input processes over the causal relationship $X \rightarrow Y$. The quantity $CP_{X \rightarrow Y|Z}$ can be easily generalized by considering vector regression models computed in $\Omega_{XYZ}=\{X, Y, \mathbf{Z}\}$ and in $\Omega_{XY}=\Omega_{XYZ} \setminus \{\mathbf{Z}\}$ respectively. The difference $CP_{X \rightarrow Y} - CP_{X \rightarrow Y|Z}$ holds the interpretation provided at the end of *Sect.III* because a positive difference indicates that the set of Z_k processes reduces the predictive ability of X about the future evolution of Y , while a negative difference indicated the opposite situation. Since (9) holds when Z is a vector variable \mathbf{Z} , leading to the computation of $IP(Y; X, \mathbf{Z})$, the proposed procedure for testing C/S is still valid.

III. SIMULATIONS AND SURROGATE DATA GENERATION

A. Simulations

Net redundancy/synergy was computed by simulating US, CD and M schemes according to the model

$$\begin{aligned} X_n &= g \cdot X_{n-1} + d \cdot Z_{n-1} + W_n^X \\ Y_n &= a \cdot Y_{n-1} + b \cdot X_{n-1} + c \cdot Z_{n-2} + W_n^Y \\ Z_n &= e \cdot X_{n-1} + f \cdot Y_{n-1} + W_n^Z \end{aligned} \quad (13)$$

where W_n^X , W_n^Y , and W_n^Z are current states of zero mean and unit variance Gaussian noises W^X , W^Y and W^Z , respectively. US, CD and M schemes were simulated while varying the strength b of the causal action from X to Y from -0.5 to $+0.5$ in steps of 0.05 and with $a=0.5-2 \cdot |b|$ and $g=0.5$. US was simulated by setting $c \neq 0.0$, $d=0.0$, $e=0.0$, and $f=0.0$. To better understand the consequence of an unbalance between the strength and phase of the actions of Z and X on Y , c was set to -1.0 , -0.5 , $+0.5$ and $+1.0$. CD was simulated by setting $c \neq 0.0$, $d \neq 0.0$, $e=0.0$ and $f=0.0$. To better appreciate the effect of altering the phase of influences of Z over X and Y , all the possible combinations with $c=\pm 0.3$ and $d=\pm 1.0$ were considered. M was simulated by setting $c \neq 0.0$, $d=0.0$, $e \neq 0.0$ and $f=0.0$. To assess the consequence of altering the sign of the M pathway compared to that from X to Y , all the possible combinations with $c=\pm 1.0$ and $e=\pm 1.0$ were considered. Twenty realizations of X , Y and Z of 256 samples were generated by considering different realizations of Gaussian white noises obtained by varying their seed. Results were reported as function of b as median and confidence interval derived from 2.5th and 97.5th percentiles. The net redundancy/synergy was computed using (9) and the true values of the parameters, starting from the different realizations of the process defined in (13).

B. Surrogate Data

Over experimental series the significance of the net redundancy/synergy balance was tested against a situation of full uncoupling among all the systems that theoretically would lead to $IP(Y; X, Z)=0.0$. In order to destroy any causal

interaction while preserving as much as possible the other statistical properties of X , Y and Z such as distribution, power spectrum and self-entropy of all considered processes, surrogate data are generated according to a time shifting procedure leading to values at the end of the sequence wrapped to their onset [30], [31]. Realizations of X and Z were time shifted according to a randomly chosen delay much larger than the maximal order of the model (i.e. 40 cardiac beats). Attention was paid that the absolute value between the two delays was longer than 40 cardiac beats as well. The original realization of Y was kept untouched. For each original triplet we generated one triplet of surrogate series. $IP(Y; X, Z)$ was computed over the set of surrogates and the 2.5th and 97.5th percentiles of the distribution of $IP(Y; X, Z)$ were extracted in each experimental condition. These critical values were labeled $IP_{S,2.5}$ and $IP_{S,97.5}$ respectively. If $IP(Y; X, Z)$ computed over the original series in a given subject in an assigned experimental condition was found below $IP_{S,2.5}$ or above $IP_{S,97.5}$, the role of Z over the causal link from X to Y could be identified. More specifically, if $IP(Y; X, Z)$ was below $IP_{S,2.5}$, Z was a S, while Z was a C if $IP(Y; X, Z)$ was above $IP_{S,97.5}$. The percentage of subjects with Z classified as S, or C, was monitored in each experimental condition and indicated as S% and C%.

IV. EXPERIMENTAL PROTOCOLS AND DATA ANALYSIS

The role played by R on the CV and CBV interactions was assessed in two different experimental protocols carried out, respectively, in a group of pathological individuals undergoing recordings before (PRE) and after (POST) general anesthesia induction with propofol and remifentanyl [12], [13], and in a group of healthy subjects undergoing recordings at rest in supine position (REST) and during postural challenge induced by head-up tilt (HUT) [14], [15].

A. PRE-POST Experimental Protocol

Data were collected in patients scheduled for coronary artery bypass grafting at the Department of Cardiothoracic, Vascular Anesthesia and Intensive Care of IRCCS Policlinico San Donato, San Donato Milanese, Milan, Italy. Details about the PRE-POST experimental protocol can be found in [12], [13]. Briefly, we studied 17 pathological subjects (age: 64 ± 8 yrs, 17 males). The inclusion criteria, ethical committee approval from San Raffaele Hospital, Milan, Italy (approval number: 40/int/2016), agreement with the principles of the Declaration of Helsinki and informed consent process were described in [12], [13]. The subjects received first premedications such as intramuscular administration of atropine (0.5 mg) and fentanyl (100 μ g). General intravenous anesthesia was induced with a bolus of propofol of 1.5 $\text{mg} \cdot \text{kg}^{-1}$ and maintained with a propofol dose of 3 $\text{mg} \cdot \text{kg}^{-1} \cdot \text{h}^{-1}$ and remifentanyl at a rate from 0.05 to 0.5 $\mu\text{g} \cdot \text{kg}^{-1} \cdot \text{min}^{-1}$ with a mean rate 0.32 $\mu\text{g} \cdot \text{kg}^{-1} \cdot \text{min}^{-1}$. Electrocardiogram (ECG) and arterial pressure (AP), invasively derived from a catheter inserted into the radial artery, were recorded from the patient's

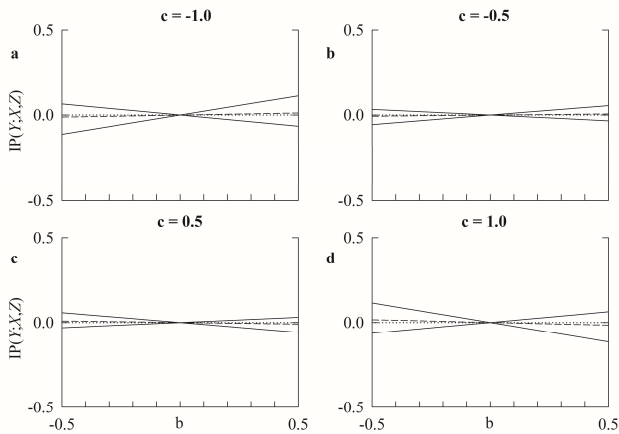


Fig.3. The line plots show $IP(Y;X,Z)$ computed over simulated data in US configuration as a function of the strength b of the causal relationship from X to Y . Results are reported according to $c=-1.0$ (a), $c=-0.5$ (b), $c=+0.5$ (c), and $c=+1.0$ (d). The solid lines are relevant to the 2.5th and 97.5th percentiles, while the dashed one to the median computed over the entire set of simulations. The dotted line denotes $IP(Y;X,Z)=0.0$.

monitor and acquired with an analog-to-digital board (National Instruments, Austin, TX, USA) connected to a laptop synchronously with cerebral blood flow (CBF) velocity measured from the middle cerebral artery via a transcranial Doppler ultrasound device (Multi-Dop X, DWL, San Juan Capistrano, CA, USA). Signals were sampled at a frequency of 1 kHz. Signals were recorded for 10 min in PRE and POST when the target plasma concentration of propofol was expected to be around $3 \mu\text{g}\cdot\text{kg}^{-1}$ based on the pharmacokinetic properties of the drug. POST session was recorded just before opening the chest. Patients spontaneously breathed during PRE and were mechanically ventilated during POST under volume-controlled mode at a rate from 12 to 16 breaths $\cdot\text{min}^{-1}$.

B. REST-HUT Experimental Protocol

Data were collected at the Neurology Division of Sacro Cuore Hospital, Negrar, Italy. Details of the REST-HUT experimental protocol can be found in [14], [15]. The

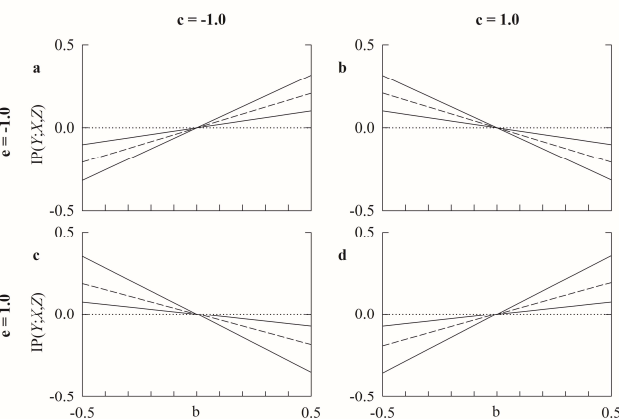


Fig.5. The line plots show $IP(Y;X,Z)$ computed over simulated data in M configuration as a function of the strength b of the causal relationship from X to Y . Results are reported according to $e=-1.0$ and $c=-1.0$ (a), $e=-1.0$ and $c=+1.0$ (b), $e=+1.0$ and $c=-1.0$ (c), and $e=+1.0$ and $c=+1.0$ (d). The solid lines are relevant to the 2.5th and 97.5th percentiles, while the dashed one to the median computed over the entire set of simulations. The dotted line denotes $IP(Y;X,Z)=0.0$.

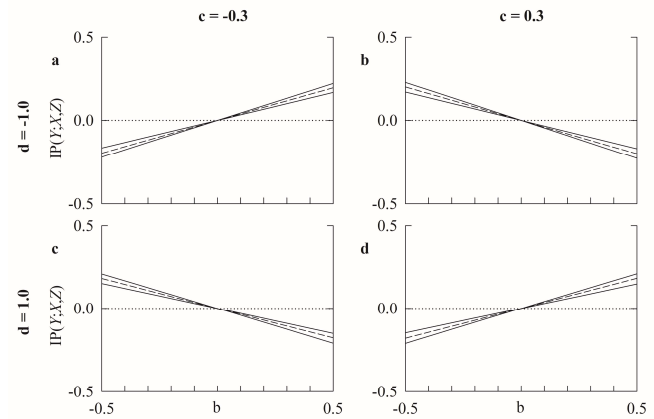


Fig.4. The line plots show $IP(Y;X,Z)$ computed over simulated data in CD configuration as a function of the strength b of the causal relationship from X to Y . Results are reported according to $d=-1.0$ and $c=-0.3$ (a), $d=-1.0$ and $c=+0.3$ (b), $d=+1.0$ and $c=-0.3$ (c), and $d=+1.0$ and $c=+0.3$ (d). The solid lines are relevant to the 2.5th and 97.5th percentiles, while the dashed one to the median computed over the entire set of simulations. The dotted line denotes $IP(Y;X,Z)=0.0$.

inclusion criteria, ethical committee approval from Sacro Cuore Hospital, Negrar, Italy (approval number: 101/2010), agreement with the principles of the Declaration of Helsinki and informed consent process were described in [14], [15].

Briefly, we considered 13 healthy control subjects (age: 27 ± 8 yrs; 5 males) with no history of syncope in the previous 2 years. Their healthy status was assessed via physical examination and full neurological assessment. Subjects were instructed to avoid caffeinated and alcoholic beverages for 24h before the study. Experiments took place in the morning in a temperature-controlled room. Subjects were instrumented to continuously monitor the ECG (lead II), AP via a volume clamp device from the middle finger of the right hand (Finapres Medical Systems, Enschede, The Netherlands) and thoracic movements through a piezoelectric belt (Marazza, Monza, Italy). The CBF velocity was measured from the middle cerebral artery through a transcranial Doppler device (Multi-Dop T, DWL, San Juan Capistrano, CA, USA).

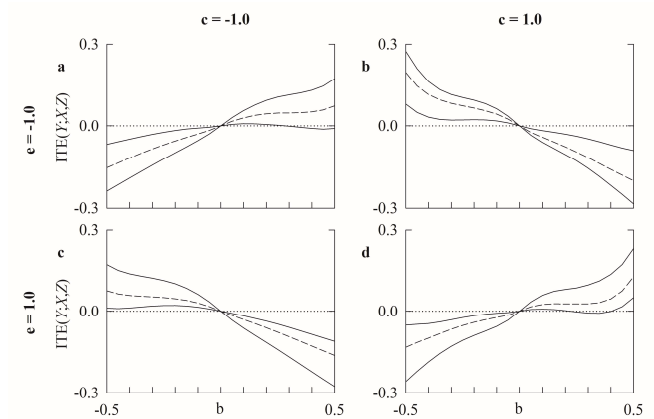


Fig.6. The line plots show $ITE(Y;X,Z)$ computed over simulated data in M configuration as a function of the strength b of the causal relationship from X to Y . Results are reported according to $e=-1.0$ and $c=-1.0$ (a), $e=-1.0$ and $c=+1.0$ (b), $e=+1.0$ and $c=-1.0$ (c), and $e=+1.0$ and $c=+1.0$ (d). The solid lines are relevant to the 2.5th and 97.5th percentiles, while the dashed one to the median computed over the entire set of simulations. The dotted line denotes $ITE(Y;X,Z)=0.0$.

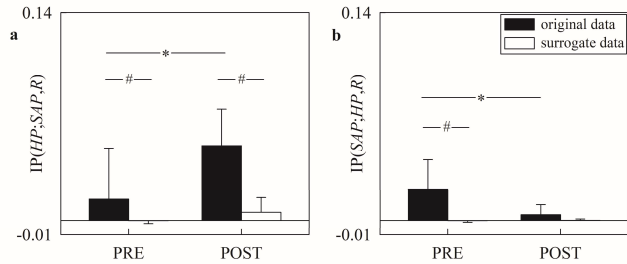


Fig.7. The grouped bar graphs show $IP(HP;SAP,R)$ (a) and $IP(SAP;HP,R)$ (b) as a function of the experimental condition in the PRE-POST protocol. Markers are computed over the original (solid black bars) and surrogate (solid white bars) data. The symbol * indicates a significant difference across experimental conditions within the same type of series, while the symbol # denotes a significant difference between original series and surrogates within the same experimental condition.

The signals were acquired synchronously at a sampling rate of 1 kHz. After having instrumented the subject, a period of 5 minutes was left for stabilization of the physiological variables. The subjects underwent 10 minutes of recording at REST and during successive HUT with tilt table inclination of 60°. No subjects exhibited signs of presyncope during HUT.

C. Beat-to-beat Series Extraction

ECG, AP and CBF were low-pass filtered with cut-off frequencies of 250, 50 and 10 Hz respectively. HP was computed from the ECG as the time interval between two consecutive R-wave peaks. The k th SAP was defined as the maximum AP value within the k th HP. Diastolic AP (DAP) was detected as the minimum AP value after the k th SAP. The k th MAP was computed as the ratio of the definite integral of AP between the $(k-1)$ th and k th DAP occurrences to the interdiastolic interval. The same procedure was applied to CBF velocity to compute the k th MCBF velocity and the fiducial points for the computation of the definite integral were the same as for the calculation of MAP [14], [15]. In the PRE-POST protocol the R series was obtained from the respiratory-related amplitude modulation of the ECG as the amplitude of the first R-wave delimiting the k th HP. In the REST-HUT protocol the R series was obtained by sampling thoracic movement signal at the first R-wave delimiting the k th HP. Missing values owing to overlooked detections of the R-wave peak were manually inserted. Misdetections linked to the occasional spikes of noise on the ECG trace were deleted. If an HP could be measured, the associated SAP, MAP, R and MCBF values were always extracted. The effect of ectopic

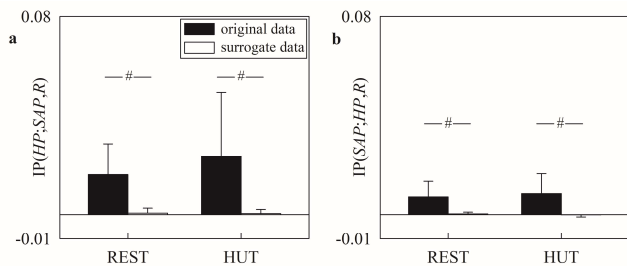


Fig.9. The grouped bar graphs show $IP(HP;SAP,R)$ (a) and $IP(SAP;HP,R)$ (b) as a function of the experimental condition in the REST-HUT protocol. Markers are computed over the original (solid black bars) and surrogate (solid white bars) data. The symbol # denotes a significant difference between original series and surrogates within the same experimental condition.

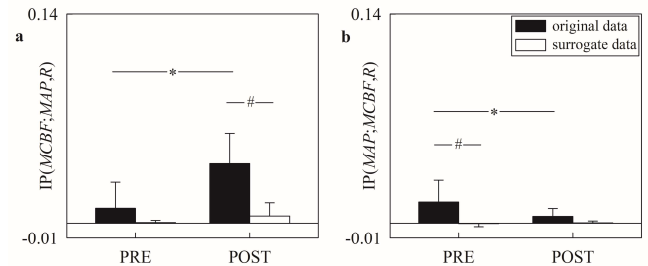


Fig.8. The grouped bar graphs show $IP(MCBF;MAP,R)$ (a) and $IP(MAP;MCBF,R)$ (b) as a function of the experimental condition in the PRE-POST protocol. Markers are computed over the original (solid black bars) and surrogate (solid white bars) data. The symbol * indicates a significant difference across experimental conditions within the same type of series, while the symbol # denotes a significant difference between original series and surrogates within the same experimental condition.

beats or isolated arrhythmic events was mitigated via linear interpolation between the closest values unaffected by arrhythmic beat. Corrections did not exceed 5% of the total sequence length. In order to study short-term regulatory mechanisms, we selected sequences of 250 consecutive synchronous HP, MAP, SAP, R and MCBF values [32] at random positions within experimental sessions. Stationarity test was applied to avoid analysis over sequences with unstable mean and variance [33]. Time domain analysis was reported in [13] and in [34] for the PRE-POST and REST-HUT protocols respectively.

D. Model Identification Procedure over Variability Series

The coefficients of the models were identified via traditional least squares approach and Cholesky decomposition method [5], [23], [24]. The delays from SAP to HP, from HP to SAP, from MAP to MCBF, from MCBF to MAP was set to 0, 1, 2 and 0 beats [12], [13]. The model order was optimized in the range from 4 to 16 according to the Akaike figure of merit for multivariate processes over the most complex model structure (i.e. the model identified in Ω_{XYZ}). The optimal model order was denoted with p_O and reported in Appendix. The model coefficients were estimated again in Ω_{XY} , Ω_{YZ} and Ω_Y while keeping the model order optimized in Ω_{XYZ} . The goodness of fit ρ was computed as the fraction of variance explained by the optimal model and reported in Appendix. ρ ranges from 0 to 1 where 0 and 1 indicate null and perfect fitting respectively.

E. Statistical Analysis

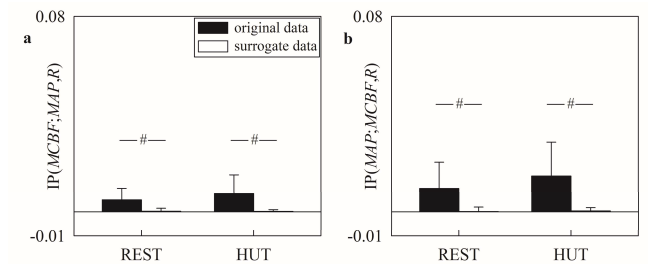


Fig.10. The grouped bar graphs show $IP(MCBF;MAP,R)$ (a) and $IP(MAP;MCBF,R)$ (b) as a function of the experimental condition in the REST-HUT protocol. Markers are computed over the original (solid black bars) and surrogate (solid white bars) data. The symbol # denotes a significant difference between original series and surrogates within the same experimental condition.

Two-way repeated measures analysis of variance (two factor repetition, Holm-Sidak test for multiple comparison) was utilized to assess the significance of the differences between original and surrogate series within the same experimental condition and between experimental conditions within the same type of data (i.e. original or surrogate series). Experimental data are reported as mean \pm standard deviation. Statistical analysis was performed with a commercial statistical software (Sigmaplot v.14.0, Systat Software, San Jose, CA, USA). A value of type I error probability $p < 0.05$ was always deemed as significant.

V. RESULTS

A. Results over Simulations

Figure 3 shows the $IP(Y;X,Z)$ monitored as a function of the strength b of the causal relationship from X to Y in the case of the US scheme. Results are given with c equal to -1.0 (Fig.3a), -0.5 (Fig.3b), $+0.5$ (Fig.3c) and $+1.0$ (Fig.3d). The dashed line is relevant to the median of $IP(Y;X,Z)$ computed over the entire set of simulations, while the solid lines to 2.5th and 97.5th percentiles. Dotted line indicates $IP(Y;X,Z)=0.0$. As expected, the median value of $IP(Y;X,Z)$ lay around 0. Dispersion tended to grow with the absolute values of b and c .

Figure 4 has the same structure as Fig.3 but shows the $IP(Y;X,Z)$ in the case of the CD scheme. Results are given with d and c equal to -1.0 and -0.3 (Fig.4a), to -1.0 and $+0.3$ (Fig.4b), to $+1.0$ and -0.3 (Fig.4c) and to $+1.0$ and $+0.3$ (Fig.4d). $IP(Y;X,Z)$ was linearly related to modifications of b and the transition from negative to positive $IP(Y;X,Z)$ values or *vice versa* occurred at $b=0$. Dispersion of $IP(Y;X,Z)$ was limited and was weakly influenced by the absolute value of b .

Figure 5 has the same structure as Fig.3 but shows the $IP(Y;X,Z)$ in the case of the M scheme. Results are given with e and c equal to -1.0 and -1.0 (Fig.5a), to -1.0 and $+1.0$ (Fig.5b), to $+1.0$ and -1.0 (Fig.5c) and to $+1.0$ and $+1.0$ (Fig.5d). Like in the CD configuration, in the M scheme $IP(Y;X,Z)$ was linearly related to b and the straight line intersected the x-axis in correspondence to $b=0$. Dispersion of $IP(Y;X,Z)$ increased remarkably with the absolute value of b .

Similarly to the Fig.5, the Fig.6 shows the results relevant to the M scheme. Net redundancy/synergy balance was computed in the TE decomposition framework via the $ITE(Y;X,Z)$. The simultaneous monitoring of $IP(Y;X,Z)$ in Fig.5 and $ITE(Y;X,Z)$ in Fig.6 over the same simulation is intended to favor the comprehension of subtle differences among these net redundancy/synergy balance metrics. The logarithm transformation was responsible for the nonlinear trend visible in all the panels (Figs.6a,b,c,d) as well as for the greater departures of $ITE(Y;X,Z)$ from x-axis when the values of $ITE(Y;X,Z)$ were negative compared to positive ones.

B. Results over Experimental Data

The group bar graphs of Fig.7 show $IP(HP;SAP,R)$ (Fig.7a) and $IP(SAP;HP,R)$ (Fig.7b) in the PRE-POST protocol. Results are given over the original series (solid black bars) and surrogates (solid white bars). Over the original series general

anesthesia increased $IP(HP;SAP,R)$, while no effect was observed over surrogates (Fig.7a). Regardless of the experimental condition $IP(HP;SAP,R)$ was significantly reduced over surrogates compared to the original data (Fig.7a). General anesthesia reduced $IP(SAP;HP,R)$ over the original data but left unmodified $IP(SAP;HP,R)$ over the surrogates (Fig.7b). $IP(SAP;HP,R)$ computed over original and surrogate data was different in PRE but not in POST condition (Fig.7b). R had a C effect for the causal link from SAP to HP in 53% and 82% of the subjects in PRE and POST respectively, while R had a S influence in 6% and 0%. R was a confounder for the causal link from HP to SAP in 76% and 47% of the subjects in PRE and POST respectively, while R was a suppressor in 0% and 0%.

Figure 8 has the same structure as Fig.7 but it shows $IP(MCBF;MAP,R)$ (Fig.8a) and $IP(MAP;MCBF,R)$ (Fig.8b). Over the original series $IP(MCBF;MAP,R)$ increased during POST, while the effect of general anesthesia was not visible over surrogates (Fig.8a). $IP(MCBF;MAP,R)$ was significantly reduced in surrogates solely in POST session (Fig.8a). Over the original data $IP(MAP;MCBF,R)$ was smaller in POST than in PRE but no PRE-POST changes were observed over the surrogates (Fig.8b). Surrogate data exhibited smaller $IP(MAP;MCBF,R)$ values compared to the original series exclusively in PRE session (Fig.8b). R had a C effect for the causal link from MAP to MCBF in 41% and 76% of the subjects in PRE and POST respectively, while R had a S influence in 12% and 0%. R was a confounder for the reverse causal pathway (i.e. MCBF to MAP) in 71% and 71% of the subjects in PRE and POST respectively, while R was a suppressor in 0% and 0%.

The group bar graphs of Fig.9 show $IP(HP;SAP,R)$ (Fig.9a) and $IP(SAP;HP,R)$ (Fig.9b) in the REST-HUT protocol. Results are given over the original series (solid black bars) and surrogates (solid white bars). Regardless of the type of data (i.e. original or surrogate series) postural stimulus left unmodified $IP(HP;SAP,R)$ (Fig.9a). The same conclusion held over $IP(SAP;HP,R)$ (Fig.9b). Regardless of the experimental condition (i.e. REST or HUT) and type of monitored variable [i.e. $IP(HP;SAP,R)$ or $IP(SAP;HP,R)$], IP was larger over the original data than in surrogates (Figs.9a,b). R had a C effect for the causal link from SAP to HP in 77% and 100% of the subjects at REST and during HUT respectively, while R had a S influence in 0% and 0%. R was a confounder for the causal link from HP to SAP in 77% and 85% of the subjects at REST and during HUT respectively, while R was a suppressor in 0% and 0%.

Figure 10 has the same structure as Fig.9 but it shows $IP(MCBF;MAP,R)$ (Fig.10a) and $IP(MAP;MCBF,R)$ (Fig.10b). Regardless of the monitored variable [i.e. $IP(MCBF;MAP,R)$ or $IP(MAP;MCBF,R)$] (Figs.10a,b), no significant differences were found between experimental conditions (i.e. REST versus HUT), while significant variations were observed between the two types of series (i.e. original data versus surrogates). R had a C effect for the causal link from MAP to MCBF in 62% and 77% of the subjects in PRE and POST respectively, while R had a S influence in 0% and 0%. R was a

confounder for the reverse causal pathway (i.e. MCBF to MAP) in 77% and 77% of the subjects in PRE and POST respectively, while R was a suppressor in 15% and 0%.

VI. DISCUSSION

The main methodological findings of this study can be summarized as follows: i) we propose a test based on the computation of the net redundancy/synergy balance to test C/S; ii) the C/S test can exploit metrics computed in the predictability and TE frameworks, even though subtle differences are present; iii) the proposed C/S test needs some *a priori* knowledge to distinguish among specific causal structures usually of interest in practical applications.

The main experimental findings of this study can be summarized as follows: i) R behaves as a confounder of the CV variability interactions and the relevance of the C role depends on the experimental challenge; ii) similar conclusions hold for the role of R on CBV variability interactions.

A. Testing C/S via Net Redundancy/Synergy Balance

This study demonstrates that testing the sign of the net redundancy/synergy balance allows the classification of the influence of a third variable on the causal relationship from source to target. Indeed, the sign of the net redundancy/synergy balance can distinguish a situation in which the knowledge of the third variable decreases the strength of the causal relationship from source to target, namely C, from a situation in which the observation of a third variable improves the ability of source in predicting target future evolution, namely S. More precisely, in C the net redundancy/synergy balance is positive, while it is negative in S. Given that the net redundancy/synergy is symmetric under reversal of the role of the two input variables, exchanging the third variable with the source does not modify conclusions. When considering the influences of two sources on a target the net redundancy/synergy balance is commonly utilized to evaluate the redundant/synergistic character of the two input variables in predicting the target behavior [4], [8]-[11], [25]-[29]. A positive value of the net redundancy/synergy balance indicates that the two sources, when observed individually, allow a more informative comprehension of the behavior of the target compared to their joint observation, namely a dominant redundancy resulting from a certain amount of shared information between sources about target effects. Conversely, a negative value indicates the opposite situation with a prevalent synergy indicating that the two sources exhibited some complementary information about the target effects. Therefore, the possibility of using the net redundancy/synergy balance to test C/S allows us to place side by side two interpretations of net redundancy/synergy balance: the more usual interpretation as a measure of the different ability of two variables in predicting the target when observed individually compared to when observed together is accompanied by the additional interpretation as a measure of the capacity of the third conditioning variable to modify the ability of a source in predicting the target. Simulations proved that C/S effects of a third variable on an input-output

relationship could be generated via a very simple model structure under different causal configurations (i.e. US, CD and M).

B. Differences in Performing the C/S Test via Predictability and TE Decomposition Frameworks

The C/S test was developed using a metric of net redundancy/synergy balance defined in the predictability decomposition framework such as IP [9], [10], but it holds even using an analog metric in the TE decomposition framework such as ITE [4], [8] [10], [11], [27]-[29]. However, the careful comparison of Fig.5 with Fig.6 clearly indicates the C/S test exploiting the definition of ITE might be biased toward an excess of S detection. Indeed, the nonlinear nature of the logarithmic function featuring steeper slopes for values of the argument smaller than 1 and smoother slopes for values of the argument larger than 1 leads to the magnification of the departures below 0 with respect to those above 0. This effect of the logarithm is responsible for the bias toward negative values of ITE in the case of US in theoretical studies [4], [8] and for a greater percentage of subjects showing synergy based on ITE than IP in experimental data [10].

C. The C/S Test Is Useless in Identifying Specific Causal Structures

While the proposed C/S test distinguishes between C and S, this study demonstrates that it cannot be fruitfully exploited to identify peculiar causal structures. For example, given two common causal schemes such as CD and M, simulations proved that CD and M cannot be distinguished because they led to both positive and negative values of IP (Figs.4,5). Even the situation of US, theoretically leading to null values of IP, could be distinguished from CD and M exclusively in statistical sense. Indeed, in the US scheme IP values different from 0 were found due to the variability of prediction errors linked to the use of different noise realizations (Fig.3). More remarkably, the magnitude of the IP departures from 0 depended on the model parameters (Fig.3), thus introducing an additional difficulty to separate US from CD and M. Therefore, we conclude that, without some extra physiological information, it is impossible to privilege a causal variability interaction structure with respect to another with the exclusive use of IP.

D. R Is a Confounder for CV Variability Interactions and the Relevance of the C Role Depends on the Experimental Challenge

Since $IP(HP;SAP,R)$ and $IP(SAP;HP,R)$ were significantly different from uncoupled surrogates and significantly above 0 in a sizable fraction of subjects regardless of the protocol and experimental condition, R is a C for the CV variability interactions. R is so powerful in disturbing directly or indirectly cardiac and vascular controls that it is not surprising to find out that accounting for R reduces the strength of the causal relationship from SAP to HP and *vice versa* [35]. Therefore, we recommend recording R in any experimental session devoted to elucidating CV regulation [36]-[38] and to include R in any model describing the CV variability

interactions [12], [16]-[18], [39]-[44]. This result is in agreement with previous studies that detected at REST an excess of redundancy of SAP and R and of HP and R in predicting HP and SAP respectively [10], [11], [45]. The dominant presence of redundancy of R was observed even in bivariate applications at the level of cardiorespiratory control, especially whether the respiratory drive was empowered via controlled breathing [46].

The C effect of R on the causal relationship from SAP to HP increased during general anesthesia. This result is the likely consequence of the powerful action of mechanical ventilation that induces periodical modifications of the intrathoracic pressure modulating venous return to the right atrium and, consequently, left ventricular stroke volume and SAP [31], [47]-[49]. Fluctuations of SAP at the ventilatory rate can induce HP changes at the same frequency via the activity of a residual baroreflex [12]. Conversely, over the reverse causal direction (i.e. from HP to SAP) the C role of R diminishes because the residual respiratory oscillations of HP are less importantly transferred to SAP due to dramatic reduction of the gain of the mechanical feedforward pathway [12] resulting from a depressed sympathetic control, reduced cardiac contractility and profound vasodilation [12], [50]-[56].

HUT did not modify the role of R over the CV variability interactions. Indeed, IP remained unvaried during the orthostatic challenge. This finding is in disagreement with [10] who suggested that the vagal withdrawal, reducing the amount of HP changes at the respiratory rate, and the decrease of the baroreflex gain [57]-[59] could explain the reduction of redundancy of R and HP over SAP and of R and SAP over HP respectively observed during HUT [10]. However, in the present study the limited tilt table inclination (i.e. 60°) might have induced an insufficient modification of vagal and baroreflex controls to cause a significant variation of IP.

E. R Is a Confounder for CBV Variability Interactions and the Relevance of the C Role Depends on the Experimental Challenge

Since $IP(MCBF;MAP,R)$ and $IP(MAP;MCBF,R)$ were above the level set by uncoupled surrogates and significantly larger than 0 in a relevant fraction of individuals in both protocols, R plays the C role for the CBV variability interactions. The finding that accounting for R reduces the strength of the causal relationship from MAP to MCBF and *vice versa* cannot be taken for granted *a priori*. Indeed, the series of MAP and MCBF, even though contaminated by R, exhibit important rhythmicities at frequency slower than the respiratory rate [60]. Therefore, we recommend recording R in any experimental session devoted to elucidating CBV regulation. This recommendation is particularly relevant given that CBV mechanisms were commonly assessed without recording R [19]-[22], [60]-[65]. The C role of R over CBV variability interactions might have led to an overestimation of the strength of MAP-MCBF association in time or frequency domains and this overestimation might depend on the experimental condition [65]-[68].

General anesthesia with propofol modified the role of R on

the CBV dynamic interactions. More specifically, R remains a confounder but its effect was more important on the pressure-to-flow relationship during POST compared to PRE, while it was less important on the reverse causal link. The more remarkable effect of R on the pressure-to-flow pathway might be related to more powerful effect of mechanical ventilation compared to spontaneous breathing in pacing venous return modifications [38], [47]-[49]. Conversely, the decreased relevance of measuring R when assessing the ability of MCBF in predicting MAP might be linked to the depression of the sympathetic control induced by propofol [12], [50]-[56]. that might have affected the efficiency of the Cushing reflex [34], [62], [63], [69], [70].

HUT did not alter the role of R on the CBV dynamic interactions. Indeed, the observation of R did not modify the ability of MAP in predicting MCBF. This result might be compatible with a preserved ability of CBV mechanisms to keep constant MCBF and limit its variability during HUT. The assessment of IP in a group of subjects prone to develop orthostatic syncope [34], [71], [72] or in subjects featuring the impairment of CA [73]-[75] might be helpful to verify this conjecture. HUT did not alter the role of R over the causal relationship from MCBF to MAP as well. Sympathetic activation induced by the postural challenge might have contributed to preserve the role of R on the flow-to-pressure link.

VII. CONCLUSION

We propose a C/S test to categorize the role of any vector variable that is known to disturb an input-output relationship. The test exploits the multivariate autoregressive modeling class but it can be easily turned out to be model-free because it uses the general concept of predictability improvement [1]. The application of the C/S test allowed a better characterization of the role of R over CV and CBV regulations under control condition and in response to challenges modifying the status of autonomic nervous system, such as propofol-based general anesthesia and gravitational stimulus. The C/S test might be useful to tailor modelling structures that more specifically describe the action of R over a causal relationship from a source to a target variable, to design experimental protocols capable to modify the role of R, to better characterize a pathology according to the type of the impact of R and to monitor whether countermeasures involving R are effective. We remark that the two different protocol settings might have introduced additional factors that could limit the generality of the conclusions. The class of linear parametric models utilized in this study, although frequently exploited to describe HP-SAP and MCBF-MAP dynamic relationship and exhibiting a significant goodness of fit as confirmed by this study as well, might be too broad to describe peculiar features of the underlying physiological interactions. Therefore, this class should be taken as a first attempt in modeling the physiology and future refinements should be proposed to account for the complexity of physiological interactions such as nonlinear behaviors and hysteresis phenomena. Future studies should extend this

TABLE I
OPTIMAL MODEL ORDER AND GOODNESS OF FIT FOR THE PRE-POST PROTOCOL

Index	PRE		POST	
	Original data	Surrogate data	Original data	Surrogate data
p_o for IP(HP;SAP,R)	7.47±2.32	7.82±1.85	11.59±2.62*	10.12±2.60#*
p_o for IP(SAP;HP,R)	8.47±3.06	7.65±1.87	11.59±2.50*	11.18±2.74*
p_o for IP(MCBF;MAP,R)	7.76±1.92	8.24±2.59	12.12±2.76*	10.35±2.91#*
p_o for IP(MAP;MCBF,R)	7.82±2.55	6.82±1.19	12.00±2.09*	10.76±2.86*
ρ for IP(HP;SAP,R)	0.78±0.14	0.74±0.17#	0.72±0.13	0.66±0.14#*
ρ for IP(SAP;HP,R)	0.85±0.10	0.77±0.14#	0.95±0.04*	0.93±0.06*
ρ for IP(MCBF;MAP,R)	0.84±0.10	0.81±0.13#	0.76±0.12	0.70±0.15#*
ρ for IP(MAP;MCBF,R)	0.82±0.17	0.76±0.18#	0.94±0.04*	0.92±0.06#*

IP = interactive predictability; HP = heart period; AP = arterial pressure; SAP = systolic AP; MCBF = mean cerebral blood flow; MAP= mean AP; R = respiration; p_o = optimal model order selected between 4 and 16; ρ = goodness of fit ranging from 0 to 1; PRE = before general anesthesia induction; POST = after general anesthesia induction. The symbol * indicates a significant difference across experimental conditions within the same type of series, while the symbol # denotes a significant difference between original series and surrogates within the same experimental condition.

technique to the modeling approaches present in literature [16]-[22], with a particular focus on the class of nonlinear models [1], [16], [19], [21], [22], with the aim at comparing results.

held in both experimental sessions. In the same protocol ρ remained unvaried with the orthostatic challenge regardless of the type of analysis, with the notable exception of ρ for IP(HP;SAP,R).

APPENDIX

Tables I and II report the optimal model order p_o and goodness of fit ρ of the model exploited to compute the IP in the PRE-POST and REST-HUT protocols respectively. In the PRE-POST protocol p_o increased significantly during POST compared to PRE in both original matched and surrogate unmatched pairs but no difference was observed between types of analysis within the same experimental condition. In the PRE-POST protocol ρ decreased over surrogate series compare to the original ones and this trend was evident in both experimental sessions. ρ increased for IP(SAP;HP,R) and IP(MAP;MCBF,R) in POST compared to PRE in both original matched and surrogate unmatched pairs. A tendency towards a decrease of ρ with the induction of general anesthesia was observed for both IP(HP;SAP,R) and IP(MCBF;MAP,R) regardless of the type of analysis. In REST-HUT protocol p_o did not vary either with postural challenge or type of series. The REST-HUT protocol confirmed the decrease of ρ over surrogate data compared to the original ones and this result

REFERENCES

- [1] A. Porta and L. Faes, "Wiener-Granger causality in network physiology with applications to cardiovascular control and neuroscience," *Proc. IEEE*, vol. 104, pp. 282-309, 2016.
- [2] J. T. Lizier et al., "Information decomposition of target effects from multi-source interactions: perspectives on previous, current and future work," *Entropy*, vol. 20, art. no. 307, 2018.
- [3] L. Barnett et al., "Granger causality and transfer entropy are equivalent for Gaussian variables," *Phys. Rev. Lett.*, vol. 103, art. no. 238701, 2009.
- [4] L. Faes et al., "Information decomposition multivariate systems: definitions, implementation and application to cardiovascular networks," *Entropy*, vol. 19, art. no 5, 2017.
- [5] G. Baselli et al., "Spectral decomposition in multichannel recordings based on multi-variate parametric identification," *IEEE Trans. Biomed. Eng.*, vol. 44, pp. 1092-1101, 1997.
- [6] A. Porta et al., "Implicit and explicit model-based signal processing for the analysis of short term cardiovascular interactions," *Proc. IEEE*, vol. 94, pp. 805-818
- [7] D. P. MacKinnon et al., "Equivalence of the mediation, confounding and suppression effect," *Prev. Sci.*, vol. 1, art. no. 20008, 2006.
- [8] A. B. Barrett, "Exploration of synergistic and redundant information sharing in static and dynamical Gaussian systems," *Phys. Rev. E*, vol. 91, art. no. 052802, 2015.
- [9] L. Faes, et al., "Predictability decomposition detects the impairment of

TABLE II
OPTIMAL MODEL ORDER AND GOODNESS OF FIT FOR THE REST-HUT PROTOCOL

Index	REST		HUT	
	Original data	Surrogate data	Original data	Surrogate data
p_o for IP(HP;SAP,R)	7.77±2.20	8.54±2.60	9.00±2.89	9.00±2.68
p_o for IP(SAP;HP,R)	7.69±1.49	8.24±2.42	9.00±2.08	9.08±2.02
p_o for IP(MCBF;MAP,R)	7.15±1.57	8.31±2.43	8.54±2.67	8.23±2.20
p_o for IP(MAP;MCBF,R)	7.54±1.76	7.54±2.03	7.38±1.66	7.77±1.64
ρ for IP(HP;SAP,R)	0.69±0.10	0.62±0.12#	0.84±0.11*	0.78±0.16#*
ρ for IP(SAP;HP,R)	0.86±0.09	0.82±0.09#	0.89±0.06	0.85±0.08#
ρ for IP(MCBF;MAP,R)	0.86±0.06	0.83±0.07#	0.88±0.06	0.84±0.09#
ρ for IP(MAP;MCBF,R)	0.83±0.05	0.79±0.07#	0.88±0.05	0.83±0.08#

IP = interactive predictability; HP = heart period; AP = arterial pressure; SAP = systolic AP; MCBF = mean cerebral blood flow; MAP= mean AP; R = respiration; p_o = optimal model order selected between 4 and 16; ρ = goodness of fit ranging from 0 to 1; REST = at rest in supine position; HUT = during 60° head-up tilt. The symbol * indicates a significant difference across experimental conditions within the same type of series, while the symbol # denotes a significant difference between original series and surrogates within the same experimental condition.

- brain-heart dynamical networks during sleep disorders and their recovery with treatment," *Phil. Trans. R. Soc. A*, vol. 374, art. no. 20150177, 2016.
- [10] A. Porta et al., "Quantifying net synergy/redundancy of spontaneous variability regulation via predictability and transfer entropy decomposition frameworks," *IEEE Trans. Biomed. Eng.*, vol. 64, pp. 2628-2638, 2017.
- [11] A. Porta et al., "Disentangling cardiovascular control mechanisms during head-down tilt via joint transfer entropy and self-entropy decompositions," *Front. Physiol.*, vol. 6, art. no. 301, 2015.
- [12] A. Porta et al., "Model-based causal closed loop approach to the estimate of baroreflex sensitivity during propofol anesthesia in patients undergoing coronary artery bypass graft," *J. Appl. Physiol.*, vol. 115, pp. 1032-1042, 2013.
- [13] V. Bari et al., "Impact of propofol general anesthesia on cardiovascular and cerebrovascular closed loop variability interactions," *Biomed. Signal Process. Control*, vol. 68, art. no. 102735, 2021.
- [14] L. Faes et al., "Investigating the mechanisms of cardiovascular and cerebrovascular regulation in orthostatic syncope through an information decomposition strategy," *Auton. Neurosci. Basic Clin.*, vol. 178, pp. 76-82, 2013.
- [15] V. Bari et al., "Nonlinear effects of respiration on the crosstalk between cardiovascular and cerebrovascular control systems," *Phil. Trans. R. Soc. A*, vol. 374, art. no. 20150179, 2016.
- [16] G. Nollo et al., "Evidence of unbalanced regulatory mechanism of heart rate and systolic pressure after acute myocardial infarction," *Am. J. Physiol.*, vol. 283, pp. H1200-H1207, 2002.
- [17] P. E. Hammer and J. P. Saul, "Resonance in a mathematical model of baroreflex control: arterial blood pressure waves accompanying postural stress," *Am. J. Physiol.*, vol. 288, pp. R1637-R1648, 2005.
- [18] G. Parati et al., "Closed-Loop cardiovascular interactions and the baroreflex cardiac arm: modulations over the 24 h and the effect of hypertension," *Front Physiol.*, pp. 10, art. no. 477, 2019.
- [19] R. B. Panerai et al., "Linear and nonlinear analysis of human dynamic cerebral autoregulation," *Am. J. Physiol.*, vol. 277, pp. H1089-H1099, 1999.
- [20] D. M. Simpson et al., "A parametric approach to measuring cerebral blood flow autoregulation from spontaneous variations in blood pressure," *Ann. Biomed. Eng.*, vol. 29, pp. 18-25, 2001.
- [21] G. D. Mitsis et al., "Modeling of nonlinear physiological systems with fast and slow dynamics. II. Application to cerebral autoregulation," *Ann Biomed Eng.*, vol. 30, pp. 555-565, 2002.
- [22] V. Z. Marmarelis et al., "Linear and nonlinear modeling of cerebral flow autoregulation using principal dynamic modes," *Open Biomed. Eng. J.*, vol. 6, pp. 42-55, 2012.
- [23] T. Soderstrom and P. Stoica, *System identification*, Prentice-Hall, Englewood Cliffs, NJ, 1988.
- [24] A. Porta et al., "Cardiovascular control and time domain Granger causality: insights from selective autonomic blockade," *Phil. Trans. R. Soc. A*, vol. 371, art.no. 20120161, 2013.
- [25] L. Angelini et al., "Redundant variables and Granger causality," *Phys. Rev. E*, vol. 81, art. no. 037201, 2010.
- [26] S. Stramaglia et al., "Synergetic and redundant information flow detected by unnormalized Granger causality: application to resting state fMRI," *IEEE Trans. Biomed Eng.*, vol. 63, pp. 2518-2524, 2016.
- [27] S. Stramaglia et al., "Expanding the transfer entropy to identify information circuits in complex systems," *Phys. Rev. E*, vol. 86, art. no. 066211, 2012.
- [28] D. Marinazzo et al., "Synergy as a warning sign of transitions: The case of the two-dimensional Ising model," *Phys. Rev. E*, vol. 99, art. no. 040101(R), 2019.
- [29] P. A. M. Mediano et al., "Measuring integrated information: comparison of candidate measures in theory and simulation," *Entropy*, vol. 21, art. no. 17, 2019.
- [30] R. G. Andrzejak et al., "Bivariate surrogate techniques: necessity, strengths, and caveats," *Phys. Rev. E*, vol. 68, art. no. 066202, 2003.
- [31] A. Porta et al., "Conditional self-entropy and conditional joint transfer entropy in heart period variability during graded postural challenge," *PLoS ONE*, vol. 10, art. no. e0132851, 2015.
- [32] Task Force of the European Society of Cardiology and the North American Society of Pacing and Electrophysiology, "Heart rate variability: standards of measurement, physiological interpretation and clinical use," *Circulation*, vol. 93, pp. 1043-1065, 1996.
- [33] V. Magagnin et al., "Non-stationarities significantly distort short-term spectral, symbolic and entropy heart rate variability indexes," *Physiol. Meas.*, vol. 32, pp. 1775-1786, 2011.
- [34] V. Bari et al., "Cerebrovascular and cardiovascular variability interactions investigated through conditional joint transfer entropy in subjects prone to postural syncope," *Physiol. Meas.*, vol. 38, pp. 976-991, 2017.
- [35] A. Porta et al., "Accounting for respiration is necessary to reliably infer Granger causality from cardiovascular variability series," *IEEE Trans. Biomed. Eng.*, vol. 59, pp. 832-841, 2012.
- [36] A. Angelone and N.A. Coulter, "Respiratory sinus arrhythmia: A frequency dependent phenomenon," *J. Appl. Physiol.*, vol. 19, pp. 479-482, 1964.
- [37] T. E Brown et al., "Important influence of respiration on human RR interval power spectra is largely ignored," *J. Appl. Physiol.*, vol. 75, pp. 2310-2317, 1993.
- [38] M. Elstad et al., "Cardiorespiratory interactions in humans and animals: rhythms for life," *Am. J. Physiol.*, vol. 315, pp. H6-H17, 2018.
- [39] R. I. Kitney et al., "Transient interactions between blood pressure, respiration and heart rate in man," *J. Biomed. Eng.*, vol. 7, pp. 217-224, 1985.
- [40] R. W. De Boer et al., "Hemodynamic fluctuations and baroreflex sensitivity in humans: a beat-to-beat model," *Am. J. Physiol.*, vol. 253, pp. H680-H689, 1987.
- [41] J. P. Saul et al., "Transfer function analysis of the circulation: unique insights into cardiovascular regulation," *Am. J. Physiol.*, vol. 261, pp. H1231-H1245, 1991.
- [42] G. Baselli et al., "Model for the assessment of heart period and arterial pressure variability interactions and of respiration influences," *Med. Biol. Eng. Comput.*, vol. 32, pp. 143-152, 1994.
- [43] T. J. Mullen et al., "System identification of closed-loop cardiovascular control: effects of posture and autonomic blockade," *Am. J. Physiol.*, vol. 272, pp. H448-H461, 1997.
- [44] A. Porta et al., "Model-based assessment of baroreflex and cardiopulmonary couplings during graded head-up tilt," *Comput. Biol. Med.*, vol. 42, pp. 298-305, 2012.
- [45] A. Porta et al., "Assessing the evolution of redundancy/synergy of spontaneous variability regulation with age," *Physiol. Meas.*, 38, 940-958, 2017.
- [46] A. Porta et al., "Paced breathing increases the redundancy of cardiorespiratory control in healthy individuals and chronic heart failure patients," *Entropy*, vol. 20, art. no. 949, 2018.
- [47] J. A. Innes et al., "Within-breath modulation of left ventricular function during normal breathing and positive-pressure ventilation in man," *J. Physiol.*, vol. 460, pp. 487-502, 1993.
- [48] K. Toska and M. Eriksen, "Respiration-synchronous fluctuations in stroke volume, heart rate and arterial pressure in humans," *J. Physiol.* vol. 472, pp. 501-512, 1993.
- [49] E.G. Caiani et al., "Non invasive quantification of respiratory modulation on left ventricular size and stroke volume," *Physiol. Meas.*, vol. 23, pp. 567-580, 2002.
- [50] C. S. Deutschman et al., "Changes in heart rate variability under propofol anesthesia: a possible explanation for propofol-induced bradycardia," *Anesth. Analg.*, vol. 79, pp. 373-377, 1994.
- [51] N. Kanaya et al., "Differential effects of propofol and sevoflurane on heart rate variability," *Anesthesiology*, vol. 98, pp. 34-40, 2003.
- [52] M. Maenpaa et al., "The effects of surgical levels of sevoflurane and propofol anaesthesia on heart rate variability," *Eur. J. Anaesthesiol.*, vol. 24, pp. 626-633, 2007.
- [53] T. J. Ebert et al., "Sympathetic responses to induction of anesthesia in humans with propofol or etomidate," *Anesthesiology*, vol. 76, pp. 725-733, 1992.
- [54] J. Sellgren et al., "Sympathetic muscle nerve activity, peripheral blood flows and baroreceptor reflexes in humans during propofol anesthesia and surgery," *Anesthesiology*, vol. 80, pp. 534-544, 1994.
- [55] F. Boerctel et al., "Effect of propofol on peripheral vascular resistance during cardiopulmonary bypass," *Br. J. Anaesth.*, 65, pp. 184-189, 1990.
- [56] H. Wang et al., "Spectral analysis of arterial pressure variability during induction of propofol anesthesia," *Anesth. Analg.*, vol. 82, pp. 914-919, 1996.
- [57] W. H. Cooke et al., "Human responses to upright tilt: a window on central autonomic integration," *J. Physiol.*, vol. 517, pp. 617-628, 1999.
- [58] A. Marchi et al., "Calibrated variability of muscle sympathetic nerve activity during graded head-up tilt in humans and its link with

- noradrenaline data and cardiovascular rhythms," *Am. J. Physiol.*, vol. 310, pp. R1134-R1143, 2016.
- [59] B. De Maria et al., "Characterization of the asymmetry of the cardiac and sympathetic arms of the baroreflex from spontaneous variability during incremental head-up tilt," *Front. Physiol.*, vol. 10, art. no. 342, 2019.
- [60] J. A. Claassen et al., "Transfer function analysis of dynamic cerebral autoregulation: a white paper from the international cerebral autoregulation research network," *J. Cereb. Blood Flow Metab.* vol. 36, pp. 665-680, 2016.
- [61] Y. C. Tzeng et al., "Fundamental relationships between blood pressure and cerebral blood flow in humans," *J. Appl. Physiol.*, vol. 117, pp. 1037-1048, 2014.
- [62] S. Saleem et al., "Is the Cushing mechanism a dynamic blood pressure-stabilizing system? Insights from Granger causality analysis of spontaneous blood pressure and cerebral blood flow," *Am. J. Physiol.*, vol. 315, pp. R484-R495, 2018.
- [63] E. Vaini et al., "Causality analysis reveals the link between cerebrovascular control and acute kidney dysfunction after coronary artery bypass grafting," *Physiol. Meas.*, vol. 40, art. no. 064006, 2019.
- [64] R. B. Panerai, "Cerebral autoregulation: from models to clinical applications," *Cardiovasc. Eng.*, vol. 8, pp. 42-59, 2008.
- [65] R. Zhang et al., "Autonomic neural control of dynamic cerebral autoregulation in humans," *Circulation*, vol. 106, pp. 1814-1820, 2002.
- [66] M. Reinhard et al., "Cerebral autoregulation in carotid artery occlusive disease assessed from spontaneous blood pressure fluctuations by the correlation coefficient index," *Stroke*, vol. 34, pp. 2138-2144, 2003.
- [67] D. Hori et al., "Optimal blood pressure during cardiopulmonary bypass defined by cerebral autoregulation monitoring," *J. Thorac. Cardiovasc. Surg.*, vol. 154, pp. 1590-1598, 2017.
- [68] C. A. Giller, "The frequency-dependent behavior of cerebral autoregulation," *Neurosurgery*, vol. 27, pp. 362-368, 1990.
- [69] H. Cushing, "Some experimental and clinical observations concerning states of increased intracranial tension," *Am. J. Med. Sci.*, vol. 124, pp. 375-400, 1902.
- [70] E. A. Schmidt et al., "Intracranial pressure is a determinant of sympathetic activity," *Front. Physiol.*, vol. 9, art. no. 11, 2018.
- [71] B. J. Carey et al., "Cerebral autoregulatory responses to head-up tilt in normal subjects and patients with recurrent vasovagal syncope," *Circulation*, vol. 104, pp. 898-902, 2001.
- [72] R. Zhang et al., "Deterioration of cerebral autoregulation during orthostatic stress: insights from the frequency domain," *J. Appl. Physiol.*, vol. 85, pp. 1113-1122, 1998.
- [73] J. Chen et al., "Impaired dynamic cerebral autoregulation and cerebrovascular reactivity in middle cerebral artery stenosis," *PLoS ONE*, vol. 9, art no. e88232, 2014.
- [74] S. L. Dawson et al., "Dynamic but not static cerebral autoregulation is impaired in acute ischaemic stroke," *Cerebrovasc. Dis.*, vol. 10, pp. 126-132, 2000.
- [75] R. V. Immink et al., "Impaired cerebral autoregulation in patients with malignant hypertension," *Circulation*, vol. 110, pp. 2241-2245, 2004.